FULL PAPER

Highly Efficient p-i-n and Tandem Organic Light-Emitting Devices Using an Air-Stable and Low-Temperature-Evaporable Metal Azide as an n-Dopant

By *Kyoung Soo Yook, Soon Ok Jeon, Sung-Yong Min, Jun Yeob Lee,* Ha-Jin Yang, Taeyong Noh, Sung-Kee Kang,* and *Tae-Woo Lee**

Cesium azide (CsN_3) is employed as a novel n-dopant because of its air stability and low deposition temperature. CsN_3 is easily co-deposited with the electron transporting materials in an organic molecular beam deposition chamber so that it works well as an n-dopant in the electron transport layer because its evaporation temperature is similar to that of common organic materials. The driving voltage of the p-i-n device with the CsN_3-doped n-type layer and a MoO_3-doped p-type layer is greatly reduced, and this device exhibits a very high power efficiency (57 lm W^{-1}). Additionally, an n-doping mechanism study reveals that CsN_3 was decomposed into Cs and N_2 during the evaporation. The charge injection mechanism was investigated using transient electroluminescence and capacitance–voltage measurements. A very highly efficient tandem organic light-emitting diodes (OLED; 84 cd A^{-1}) is also created using an n–p junction that is composed of the CsN_3-doped n-type organic layer/MoO_3 p-type inorganic layer as the interconnecting unit. This work demonstrates that an air-stable and low-temperature-evaporable inorganic n-dopant can very effectively enhance the device performance in p-i-n and tandem OLEDs, as well as simplify the material handling for the vacuum deposition process.

1. Introduction

Although significant progress has been made in vacuum-deposited organic light-emitting diodes OLEDs, low-voltage operation remains a crucial requirement in OLEDs in order to achieve low power consumption, which is essential for the commercialization of solid-state lighting and flat-panel displays.[1,2] Electrical doping in small-molecule-based charge transport layers has proven to be very effective for reducing the operating voltage of the device because of the increased conductivity.[2–4] The electrical doping method was applied in order to fabricate p-i-n OLED devices with very low operating voltages and high efficiencies.[2–4] The highly conductive p- and n-doped layers enhance the charge injection from the contacts and reduce the ohmic losses in these layers during the device operation.[2–4]

The typical dopants in the hole transporting layers for organic conductive p-doped layers include very strongly electron-accepting organic materials such as tetrafluoro-tetracyanoquinodimethane (F_4-TCNQ),[5] semiconducting metal oxides such as tungsten trioxide (WO_3),[6] molybdenum trioxide (MoO_3)[7] and rhenium dioxide (ReO_2),[8] and fullerene (C_{60}).[9] In general, the typical dopants that are used in the electron-transporting layers for organic conductive n-doped layers include low-work-function alkaline metals such as lithium (Li)[2,10] and cesium (Cs),[6,11] metal carbonates such as cesium carbonate (Cs_2CO_3),[4] metal nitride,[12] metal quinoline,[13] and metal fluorides such as lithium fluoride (LiF).[14] The alkaline metal n-dopants are very sensitive to oxygen and moisture, and thus their derivatives (carbonate or fluoride) are good candidates for replacing reactive metals because these materials are not sensitive to oxygen. However, most of the n-dopants that are based on alkaline metal derivatives only evaporate at temperatures that are much higher than the normal evaporation temperatures of organic materials. The co-deposition of low-temperature-evaporable organic materials and high-temperature-evaporable metal derivatives in typical thermal evaporation chambers could result in the out-gassing of the organic molecules from the chamber wall during the evaporation because of the high temperature heating. Therefore, the evaporation chambers may require frequent cleaning. Recently, molecular n-dopants without alkaline metals or their derivatives have been developed for highly power-efficient OLEDs by NOVALED AG in Germany.[15] Although the chemical structure of the molecular n-dopants has not been disclosed, they can be

[*] Prof. J. Y. Lee, K. S. Yook, S. O. Jeon
Department of Polymer Science and Engineering
Dankook University
Jukjeon-dong Suji-gu, Yongin, Gyeonggi-do, 448-701 (Korea)
E-mail: leej17@dankook.ac.kr
Prof. T.-W. Lee, S.-Y. Min
Department of Materials Science and Engineering
Pohang University of Science and Technology
San 31 Hyoja-dong, Nam-gu, Pohang, Gyeongbuk 790-784 (Korea)
E-mail: twlee@postech.ac.kr
Dr. H.-J. Yang, Dr. T. Noh, Dr. S.-K. Kang
Samsung Mobile Displays
Mt. 14-1, Nongseo-dong, Giheung-gu
Yongin-si, Gyeonggi-do 446-712 (Korea)

DOI: 10.1002/adfm.201000137

evaporated at low temperature. However, NOVALED AG is developing air-stable molecular n-dopants because its current molecular n-dopants are not stable in air. Nowadays, the development of novel low-temperature-evaporable and air-stable n-dopants is a very important issue for the formation of efficient electron injection contacts in OLEDs. Additionally, new n-dopants that are stable under ambient conditions and evaporable at low temperatures must be developed in order to easily fabricate multistack (i.e., tandem) structures for p-i-n OLEDs in real display and lighting applications.
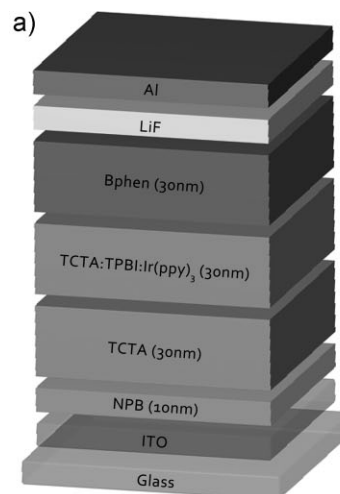
In this work, cesium azide (CsN_3) was introduced as a new n-dopant because it could be handled in air and deposited at low temperatures. CsN_3 can be co-evaporated with typical electron transporting materials in organic heating crucibles because the melting temperature of CsN_3 (310 °C) is much lower than LiF (845 °C). The CsN_3 deposition mechanism was investigated, and the device performances of the CsN_3-doped green phosphorescent devices were compared to common devices without the n-dopant. Additionally, the p-i-n structure of the green phosphorescent device was fabricated using MoO_3 as the p-dopant and CsN_3 as the n-dopant. The charge injection mechanism of the devices was investigated using the transient electroluminescence and capacitance–voltage measurements. This work demonstrated that the air-stable and low-temperature-evaporable inorganic n-dopant can very effectively enhance the device performance of the OLEDs as well as simplify the vacuum deposition process and material handling.
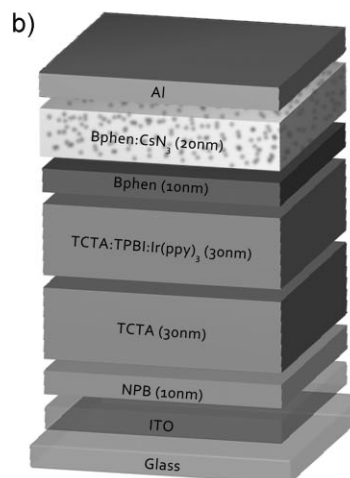
2. Results and Discussion

Cesium (Cs) is a well known n-doping material, and doping Cs in electron transport layers such as 4,7-diphenyl-1,10-phenanthroline (BPhen) has been used as an effective way of n-doping.[1] Cs has a work function of 2.3 eV, and it is a suitable n-dopant through electron transfer to Bphen, which has a lowest unoccupied molecular orbital (LUMO) of 2.8 eV. However, Cs is very reactive and sensitive to moisture and oxygen, and its use is limited because of an unstable deposition process. Therefore, a new stable Cs derivative material is required. The material must provide an n-doping effect in the electron transporting layers, while possessing the abilities to be stably evaporated at low temperatures and handled under ambient conditions without decomposition.

Instead of the direct deposition of Cs, Cs doping can be achieved through the evaporation of the material, which can liberate Cs during the deposition. Cesium azide (CsN_3) was chosen as the material to liberate Cs during the thermal deposition because it is known to decompose into Cs and N_2 when thermal energy is introduced. Additionally, CsN_3 is very stable under ambient conditions and can be deposited at low temperatures because of its low bonding energy.
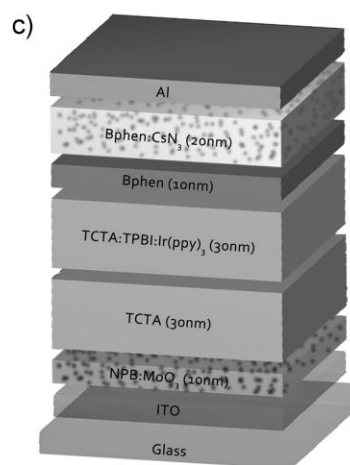
The device structures that were used in this work are shown in Figure 1. Figure 1a shows the standard device structure, which was composed of indium tin oxide (ITO, 150 nm), N,N'-di(1-naphthyl)-N,N'-diphenylbenzidine (NPB, 10 nm), 4,4',4''-tris(N-carbazolyl)-triphenylamine (TCTA, 30 nm): 1,3,5-tris(N-phenylbenzimidazole-2-yl)benzene (TPBI): tris(2-phenylpyridine) iridium (Ir(ppy)$_3$) [TCTA:TPBI = 50v:50v, 5% doping of Ir(ppy)$_3$, 30 nm], Bphen (30 nm), LiF (1 nm), and Al (200 nm). In Figure 1b, the CsN_3-doped

Figure 1. Device structures of standard, n-doped, and p-i-n devices

www.MaterialsViews.com

ADVANCED
FUNCTIONAL
MATERIALS
www.afm-journal.de

FULL PAPER

Bphen layer (n-doped layer) was employed as the electron injecting layer, and thus the Bphen (10 nm)/Bphen:CsN$_3$ (20 nm, 30%) layer was used instead of the Bphen (30 nm)/LiF (1 nm) layer. The p-i-n devices were also fabricated using MoO$_3$-doped NPB (30%) as the p-doped layer and the CsN$_3$-doped Bphen layer as the n-doped layer in Figure 1c. TCTA was employed as the exciton blocking layer in order to block exciton diffusion from the emitting layer to the hole transporting layer, and Bphen was used both as the electron transporting layer and the exciton blocking layer.

The device performances of the CsN$_3$-doped green phosphorescent OLEDs (PHOLEDs) were compared to the undoped devices, and the current density–voltage–luminance characteristics are shown in Figure 2. Figure 2a and b show that the current density of the PHOLEDs sharply increased after doping CsN$_3$ in Bphen, and the luminance was also increased by the CsN$_3$ doping. The driving voltage of the CsN$_3$-doped PHOLEDs was 3.7 V at 1000 cd m^{-2}, which was more than 1 V lower than the standard device. The low driving voltage of the CsN$_3$-doped device is due to the lowered interfacial energy barrier and the increased conductivity of the CsN$_3$-doped electron transport layer. The doped electron transport layers led to thin space charge layers and thus efficient tunneling injection despite the high barriers. The ohmic contact of the CsN$_3$-doped layer with Al was induced by the CsN$_3$-doping in Figure 3, and the improved conductivity of the CsN$_3$-doped electron transport layer was responsible for the high current density because it caused the low voltage drops in the transport layers. The conductivity of the CsN$_3$-doped Bphen layer was optimized with a maximum value of 8.1×10^{-6} S cm^{-1} at a doping concentration of 30%. Therefore, a high carrier injection level was achieved without matching the electrode work functions. The current density–voltage characteristics exhibited a linear relationship at positive and negative voltages, indicating the ohmic contact of CsN$_3$-doped Bphen with ITO and Al. The driving voltage was further reduced by doping the NPB layer with MoO$_3$. The MoO$_3$-doped NPB layer removed the interfacial energy barrier between ITO and NPB because of the ohmic contact formation at the interface. These p-i-n type device structures guaranteed an efficient carrier injection from both side contact electrodes into the doped transport layers and low ohmic losses in these highly conductive layers. Additionally, the n-doping did not affect the charge leakage in the negative bias region.

The power efficiency of the CsN$_3$-doped devices is shown in Figure 2. The MoO$_3$-doped NPB layer facilitated the hole injection from ITO because of the ohmic contact between ITO and the MoO$_3$-doped NPB layer. The power efficiency of the CsN$_3$-doped device was further improved after MoO$_3$ was doped in NPB. The power efficiencies of the n-doped and the p-i-n device were 51 and 57 lm W^{-1}, respectively, whereas the power efficiency of the standard device was 43 lm W^{-1}.

The CsN$_3$ decomposition has been reported to proceed according to the following mechanism.[13]

$$CsN_3 \rightarrow Cs + 3/2N_2 \qquad (1)$$

Therefore, CsN$_3$ was decomposed into Cs and N$_2$ and liberated Cs during the evaporation. Only Cs was deposited on the substrate during the CsN$_3$ evaporation, and it acted as an n-dopant. After the CsN$_3$ evaporation, the surface of the quartz crystal microbalance
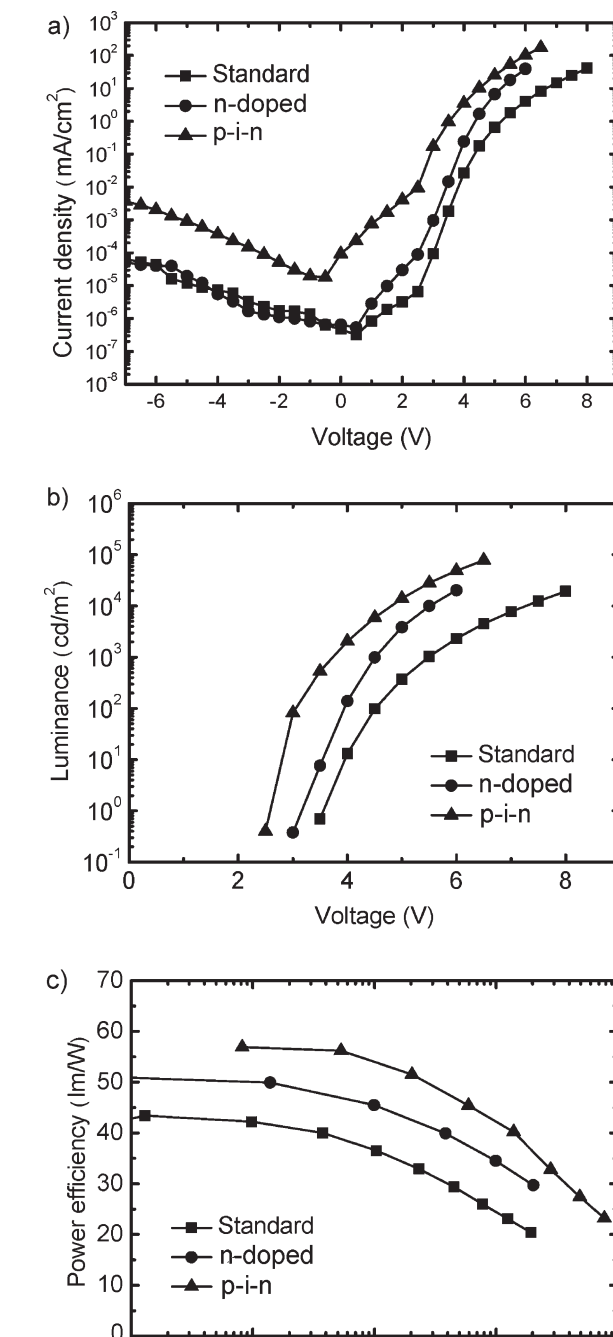

Figure 2. Current density–voltage–luminance curves of standard, n-doped, and p-i-n devices: a) current density versus voltage, b) luminance versus voltage, c) power efficiency versus luminance.

was analyzed using X-ray photoelectron spectroscopy (XPS; Fig. 4), in order to confirm the Cs deposition on the substrate. The Cs$_{3d3}$ and Cs$_{3d5}$ peaks were observed at 737.6 and 723.2 eV, respectively, and were assigned to Cs and cesium oxide. If CsN$_3$ was deposited on the quartz crystal without any decomposition, the Cs and N$_{1s}$ peaks should be observed from the XPS data. However, no peaks were observed in the N$_{1s}$ region at around 400 eV. The disappearance of the nitrogen peak in the XPS spectrum indicated
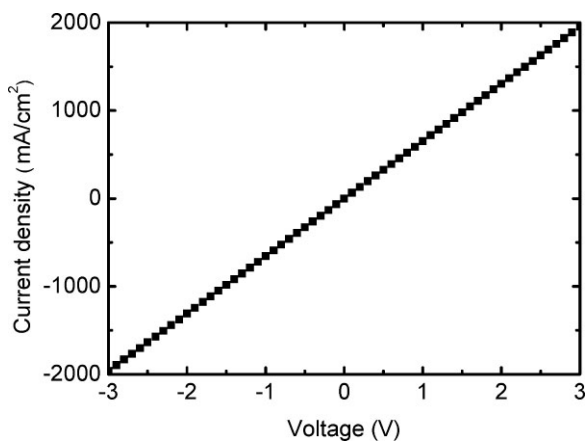
Figure 3. Current density–voltage curves of ITO/Bphen:Cs/Al single layer devices.
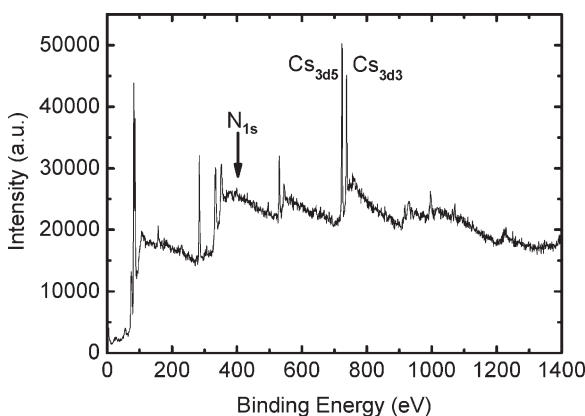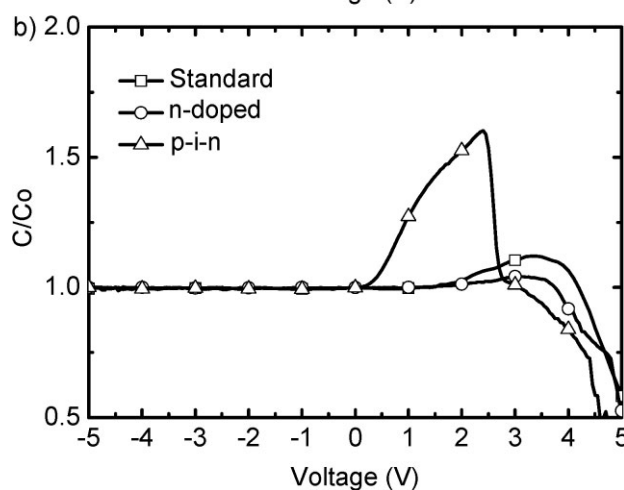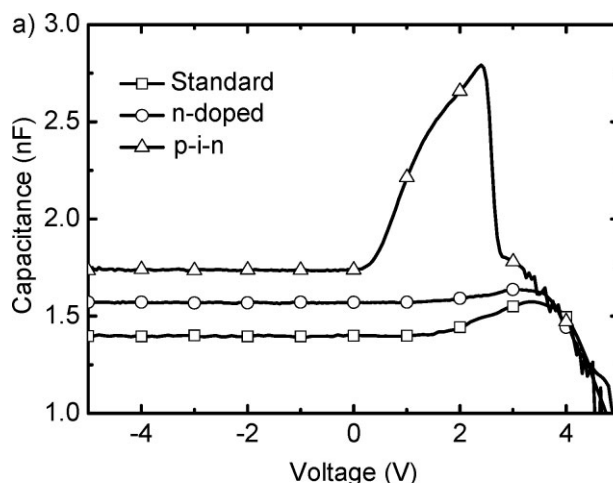

Figure 4. X-ray photoelectron spectrum of quartz crystal after CsN$_3$ deposition.
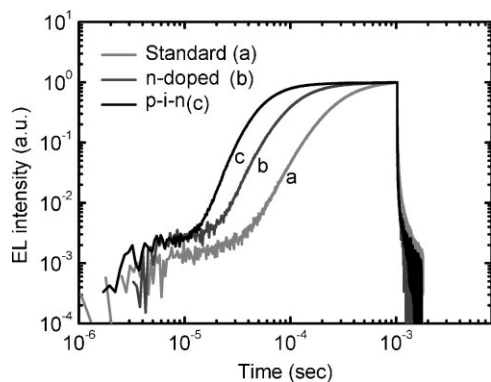

Figure 5. The capacitance–voltage characteristics of the standard, p-doped, p-i-n devices. a) The measured capacitance as a function of voltage. b) The measured capacitance normalized by the geometrical capacitance (C_0) as a function of voltage.

that only Cs, not CsN$_3$, was deposited onto the quartz crystal. The cesium oxide peak at 723.2 eV originated from partial oxidation of Cs during the transfer of the Cs-coated quartz crystal from the evaporation chamber to the analysis chamber. Therefore, CsN$_3$ was expected to have an n-doping effect through the decomposition into Cs during the film formation.

In Figure 5, the capacitance–voltage characteristics were analyzed using an ac impedance analyzer (Solartron 1260) in order to further investigate the device characteristics. The capacitance in the reverse biases was almost constant, which indicated that the geometric capacitance (C_0) was determined by the following simple equation.

$$C_0 = \varepsilon_o \varepsilon A / d \qquad (2)$$

In this equation, C_0 is the geometric capacitance, ε_o is the vacuum permittivity, ε is the dielectric constant, A is the pixel area, and d is the thickness of the organic layers between the electrodes. The C_0 of the standard, n-doped, and p-i-n devices were 1.40, 1.57, and 1.74 nF, respectively. The increase in the C_0 indicated that the doped layers did not influence the total C_0 because of the high

conductivity, which was the main reason for the lowered operating voltages of the n-doped and p-i-n devices. For the standard device, the capacitance tended to increase above 1.5 V. The capacitance continued to increase up to the device turn-on voltage ($\sim$3.5 V), where the electron–hole recombination started to take place. At the voltages below the maximum point of the capacitance, the increase in the capacitance was interpreted as the build-up of the majority charge carriers before the recombination inside the device. The main capacitance peaks corresponded to the voltage points where the majority carriers accumulated most without recombination. For the n-doped device, the capacitance at the turn-on voltage only slightly increased compared to the geometric capacitance because the major charge carriers were holes and the hole injection was not enhanced in the n-doped devices. Instead, the increased electron injection that was caused by the n-doping facilitated the charge recombination, and thus, the accumulated holes inside the device decreased accordingly, which resulted in only a slight increase in the capacitance. However, when the p-i-n device structure was designed to enhance both the hole and the electron injection, the capacitance tended to sharply increase above 0.35 V with a maximum peak at 2.4 V (i.e. the turn-on voltage) because of the

enhanced hole injection. When the injected holes and electrons were not well balanced, the capacitance tended to increase further above the turn-on voltages as reported in the literature.[16] However, for the p-i-n devices in this study, the maximum capacitance was observed exactly at the turn-on voltage, which indicated that the electrons and holes were efficiently balanced in the device. Additionally, in the p-i-n device the capacitance very abruptly dropped above the turn-on voltage in Figure 5 because of the efficient electron–hole recombination.

The transient electroluminescence measurements were performed in order to observe the effects of the doped layers on the electron–hole recombination in the device (Fig. 6). The delay time was defined as the time when the electroluminescence began to occur. The standard device exhibited a delay time of $40\,\mu s$. However, when the n-doped layer was used, the delay time was reduced to $21\,\mu s$. The p-i-n device had the shortest delay time of $12.5\,\mu s$, corresponding to a fast radiative recombination of the electrons and holes. Generally, the delay time of the transient electroluminescence shortened with increasing charge carrier mobility or conductivity of the injection or transporting layers. The device exhibited a fast electron–hole recombination rate in spite of the devices having the same total thickness because the conductivity of the hole transporting and electron transporting layers was increased through incorporation of the conductive dopant into the layers. Therefore, this type of doping strategy can be used to increase the response time of the emitting displays as well as the device efficiency.

Finally, highly efficient tandem phosphorescent OLEDs were fabricated using the n–p junction of the Bphen:CsN_3 n-doped layer and the MoO_3 p-type layer as the new interconnecting unit. The tandem device structure that was fabricated was ITO/NPB $(10\,nm)$/TCTA $(30\,nm)$/TCTA: TPBI: $Ir(ppy)_3$ $(30\,nm, 5\%$ doping)/Bphen $(10\,nm)$/Bphen:CsN_3 $(20\,nm, 20\%)$/MoO_3 $(15\,nm)$/TCTA $(30\,nm)$/TCTA: TPBI: $Ir(ppy)_3$/Bphen $(20\,nm)$/LiF/Al. Figure 7 shows the device current efficiency of the single device with a structure of ITO/NPB $(10\,nm)$/TCTA $(30\,nm)$/TCTA: TPBI: $Ir(ppy)_3$ $(30\,nm, 5\%$ doping)/Bphen $(30\,nm)$/LiF/Al and the tandem device. The luminous efficiency of the tandem device was almost doubled. A maximum device efficiency of $84\,cd\,A^{-1}$ was achieved in the tandem device, whereas the single-stack device exhibited an efficiency of $41\,cd\,A^{-1}$. These results indicated that the interconnecting unit worked very well in the tandem structure of the OLEDs.
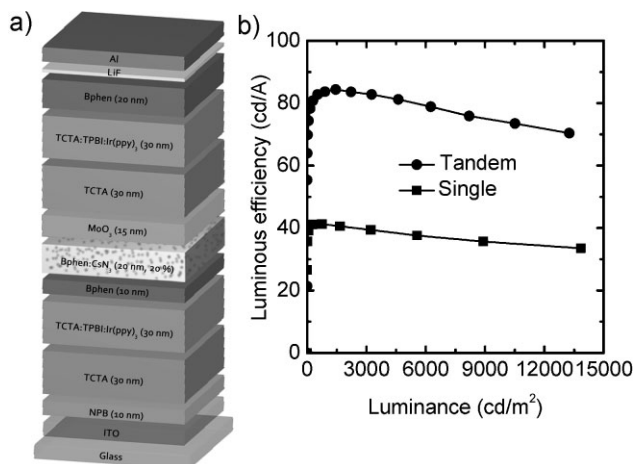
Figure 7. A tandem OLED using a new interconnecting unit composed of BPhen: CsN_3 $(20\,nm, 20\%)$/MoO_3 $(15\,nm)$. a) The device structure of the tandem OLED, and b) the luminous efficiency of the tandem OLED compared with that of the single-stack device.

3. Conclusions

A metal azide (CsN_3) was employed as an n-dopant in the electron transport layer. CsN_3 was stable under ambient conditions and was stably deposited through thermal deposition at low temperatures similar to organic materials. The n-doping effects of CsN_3 were produced through decomposition of CsN_3 during the evaporation. The driving voltage of the p-i-n device with the CsN_3-doped n-type layer and the MoO_3-doped p-type layer was greatly reduced, and the device exhibited very high power efficiency ($57\,lm\,W^{-1}$). The capacitance–voltage study showed that the holes were the main major charge carriers in the p-i-n device. Additionally, both the holes and electrons were efficiently injected and then very efficiently recombined. The transient electroluminescence study also showed that the doped layers reduced the response time of the OLED devices. This work demonstrated that this type of doping approach, using an inorganic n-type material with a low deposition temperature in the electron transport layer, was very useful and effective for enhancing the device performance in OLEDs as well as simplifying the vacuum deposition process and material handling. Finally, this work demonstrated that the CsN_3-doped n-type layer could effectively be employed in combination with a p-type layer as the interconnecting unit in tandem OLEDs, resulting in a very high luminous efficiency ($84\,cd\,A^{-1}$). As a result, this type of air-stable inorganic metal azide, which was evaporable at low temperatures, can be used to overcome the well-known drawbacks of reactive metal dopants and air-unstable organic n-dopants for high-performance p-i-n and tandem OLEDs.

4. Experimental

OLED Fabrication and Characterization: The standard device structure that was used in this experiment was ITO $(150\,nm)$/NPB $(10\,nm)$/TCTA $(30\,nm)$/TCTA: TPBI: $Ir(ppy)_3$ $(30\,nm, 5\%$ doping)/Bphen $(30\,nm)$/LiF $(1\,nm)$/Al $(200\,nm)$. The TCTA layer on top of the NPB layer was used as an exciton blocking layer in order to block the exciton diffusion from the emitting layer to the hole transport layer. The emitting layer on top of the

Figure 6. Transient electroluminescence of standard, p-doped, and p-i-n devices.

TCTA layer contained a mixed dual host of 50% TCTA and 50% TPBI through co-deposition. The Bphen layer was used as both the exciton blocking layer and electron transport layer. The CsN_3-doped devices used the Bphen (10 nm)/Bphen: CsN_3 (20 nm, 30%) layer instead of the Bphen (30 nm)/LiF layer. Al was directly deposited onto the Bphen: CsN_3 layer without the LiF layer. MoO_3-doped NPB (30%) was used as the p-doped layer in the p-i-n devices. The n–p junction of the Bphen: CsN_3 and MoO_3 films was also used as an interconnecting layer in the device structure of ITO/NPB (10 nm)/TCTA (30 nm)/TCTA: TPBI: $Ir(ppy)_3$ (30 nm, 5% doping)/Bphen (10 nm)/Bphen: CsN_3(20 nm, 20%)/MoO_3 (15 nm)/TCTA (30 nm)/TCTA: TPBI: $Ir(ppy)_3$/Bphen (20 nm)/LiF/Al. The current density–voltage–luminance characteristics of the devices were measured using a Keithley 2400 source measurement unit and a CS 1000 spectrophotometer. The CsN_3 deposition mechanism was observed using XPS. The capacitance–voltage measurements were performed using an impedance analyzer (Solartron 1260) at a constant frequency of 100 Hz with a time delay of ~6 s between the data points and an applied ac bias voltage of 50 mV.

Transient Electroluminescence Measurements: A low-duty-cycle electrical pulse (100 μs pulse width, 10 Hz pulse frequency) that was produced using an HP 8116A 50 MHz pulse/function generator was applied to the device for the transient electroluminescence measurements. The low duty cycle of the electrical pulses minimized the device heating and reduced the number of residual space charges that were present after each switch-off of the voltage pulse. The emitted light was detected using a photomultiplier tube assembly (HC125-01, Hamamatsu Corp.; rise-time: 1.5 ns). The pulse shape and the photodetector output signal were measured using an oscilloscope (Agilent Infinium 54830B oscilloscope 600 MHz 4GSa/s).

[1] S. Reineke, F. Lindner, G. Schwartz, N. Seidler, K. Walzer, B. Lüssem, K. Leo, *Nature* **2009**, *459*, 234.

[2] M. Pfeiffer, S. R. Forrest, K. Leo, M. E. Thompson, *Adv. Mater.* **2002**, *14*, 1633.

[3] K. Walzer, B. Maennig, M. Pfeiffer, K. Leo, *Chem. Rev.* **2007**, *107*, 1233.

[4] T.-W. Lee, T. Noh, B.-K. Choi, M.-S. Kim, D. W. Shin, J. Kido, *Appl. Phys. Lett.* **2008**, *92*, 043301.

[5] X. Zhou, J. Blochwitz, M. Pfeiffer, A. Nollau, T. Fritz, K. Leo, *Adv. Funct. Mater.* **2001**, *11*, 310.

[6] C.-C. Chang, M.-T. Hsieh, J.-F. Chen, S.-W. Hwang, C. H. Chen, *Appl. Phys. Lett.* **2006**, *89*, 253504.

[7] H. Ikeda, J. Sakata, M. Hayakawa, T. Aoyama, T. Kawakami, K. Kamata, Y. Iwaki, S. Seo, Y. Noda, R. Nomura, S. Yamazaki, *2006 SID Intl. Symp. Digest Tech. Pap,* Society for Information Display, Campbell, CA **2006**, p. 923.

[8] D.-S. Leem, H.-D. Park, J.-W. Kang, J.-H. Lee, J. W. Kim, J.-J. Kim, *Appl. Phys. Lett.* **2007**, *91*, 011113.

[9] J. Y. Lee, J. H. Kwon, *Appl. Phys. Lett.* **2006**, *88*, 183502.

[10] a) J. Kido, T. Matsumoto, *Appl. Phys. Lett.* **1998**, *73*, 2866. b) J. Huang, M. Pfeiffer, A. Werner, J. Blochwitz, K. Leo, S. Liu, *Appl. Phys. Lett.* **2002**, *80*, 139.

[11] a) R. Meerheim, K. Walzer, M. Pfeiffer, K. Leo, *Appl. Phys. Lett.* **2006**, *89*, 061111. b) T. Oyamada, H. Sasabe, C. Adachi, S. Murase, T. Tominaga, C. Maeda, *Appl. Phys. Lett.* **2005**, *86*, 033503.

[12] K. S. Yook, S. O. Jeon, C. W. Joo, J. Y. Lee, T.-W. Lee, T. Noh, H.-J. Yang, S.-K. Kang, *Synth. Met.* **2009**, *159*, 1664.

[13] J. Endo, T. Matsumoto, J. Kido, *Jpn. J. Appl. Phys.* **2002**, *41*, 800.

[14] K. R. Choudhury, J.-H. Yoon, F. So, *Adv. Mater.* **2008**, *20*, 1456.

[15] J. Birnstock, T. Canzler, M. Hofmann, A. Lux, S. Murano, *SID Intl. Symp. Digest Tech. Pap,* Society for Information Display, Campbell, CA **2007**, p. 1193.

[16] T.-W. Lee, J.-J. Park, Y. Kwon, T. Hayakawa, T.-L. Choi, J. H. Park, R. R. Das, M.-A. Kakimoto, *Langmuir* **2008**, *24*, 12704.